

EFFECTS OF INFLOW BOUNDARY LAYER ON TURBULENT HEAT TRANSFER  
OVER A TWO-DIMENSIONAL HILL

T. Houra

Department of Mechanical Engineering,  
Nagoya Institute of Technology  
Gokiso-cho, Showa-ku, Nagoya 466-8555, Japan  
houra@heat.mech.nitech.ac.jp

Y. Nagano

Department of Mechanical Engineering,  
Nagoya Institute of Technology  
Gokiso-cho, Showa-ku, Nagoya 466-8555, Japan  
nagano@heat.mech.nitech.ac.jp

## ABSTRACT

An experimental investigation has been made on the flow and thermal fields over a heated two-dimensional hill. The effects of the inflow boundary layer on the complex turbulent field are discussed when the downstream location of the hill model is varied. At the crest of the hill, the horizontal velocity fluctuation shows a large distinct peak very near the surface, because of instantaneous backward flows. It is found that in the reverse-flow region on the leeward side of the hill, the turbulence intensities and the Reynolds shear stress show much larger values than those in a canonical wall-bounded shear flow. The ratio of an incoming boundary layer thickness  $\delta$  to a hill height  $H$ , i.e.,  $\delta/H$ , strongly affects the development of these turbulent statistics. In the thermal field, there is a hot region below the hill height, and the mean temperature gradient has peaks at this location as well as at the heated surface. A second temperature fluctuation peak exists except near the heated surface.

## INTRODUCTION

Because environmental problems in urban areas such as the heat-island effect are becoming serious, it is necessary to clarify the heat and mass transport processes in a complex turbulent field from a fundamental viewpoint (Hunt and Snyder, 1980; Britter *et al.*, 1981; Taylor *et al.*, 1987). Although many studies on turbulent flow characteristics over a two-dimensional hill have yielded valuable results (Almeida *et al.*, 1993; Loureiro *et al.*, 2007), the detailed characteristics have not yet been fully elucidated. Moreover, few experimental data are available on a thermal field. Thus, highly accurate turbulence models for predicting such fields do not exist at present.

In the present study, we measure the flow and thermal fields over a heated two-dimensional hill to elucidate important characteristics of the complex turbulent flow. The effects of inflow turbulent boundary layer on turbulent structures formed along a separated region are discussed by varying the streamwise location of the hill model.

## EXPERIMENTAL APPARATUS

The experimental apparatus used is the same as in our previous study (Houra *et al.*, 2008). The contraction ratio of the settling chamber is 4 : 1, and the cross-sectional area

and the length of the test section are  $500 \times 500 \text{ mm}^2$  and four meters, respectively. To generate a stable turbulent boundary layer on one side of the wall, a tripping device is placed at the inlet to the test section.

A two-dimensional hill with a cosine-squared shape is installed at the test section as shown in Fig. 1. The height and width of the hill are  $H = 40 \text{ mm}$  and  $2L = 200 \text{ mm}$ , respectively. The hill's surface distance from the floor ( $y = 0$ ) is written as follows:

$$h(x) = H \cos^2 \left( \frac{\pi x}{2L} \right), \quad -1 \leq \frac{x}{L} \leq 1. \quad (1)$$

This shape has been frequently used by many investigators (Gong and Ibbetson, 1989; Ferreira *et al.*, 1991, 1995; Kim *et al.*, 1997; Ross *et al.*, 2004; Hattori and Tanaka, 2006; Wood, 1995). This is considered to be one of the typical hill shapes. Prior to the installation of the hill, the streamwise pressure gradient is set to zero. Under the present measurement condition (free-stream velocity:  $\bar{U}_0 = 8 \text{ m/s}$ ), the free-stream turbulence level is below 0.4%.

The ratio of an incoming boundary layer thickness  $\delta$  to a hill height  $H$ , i.e.,  $\delta/H$ , is an important parameter to describe the turbulent characteristics over the hill. With a view to the atmospheric boundary layer studies, the ratio would normally be set to an order of 10. On the other hand, some studies devoted to the engineering interest in the separation bubble, set the ratio to an order of one (Loureiro *et al.*, 2007). In the present study, with the focus on the tur-

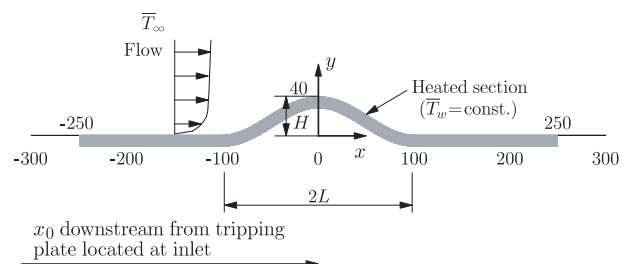


Figure 1: Two-dimensional hill with a cosine-squared shape and thermal boundary condition. Streamwise distance from tripping plate  $x_0$  is 750 mm (Case A) and 2250 mm (Case B). All dimensions are in millimeters.

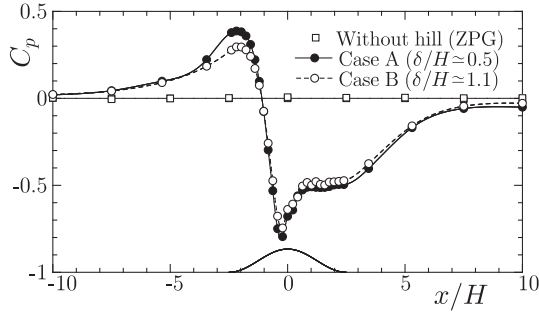


Figure 2: Static pressure distributions on surface of hill.

bulent heat transfer around the separation bubble, the ratio is set to the order one. The streamwise distance of the hill center from the inlet,  $x_0$ , is varied for two test cases: (a) Case A,  $x_0=750$  mm, and (b) Case B,  $x_0=2250$  mm. The thickness and the Reynolds number of the inflow turbulent boundary layer are different for these cases. For Case A, the boundary layer thickness of the inflow  $\delta$  and the Reynolds number based on the momentum thickness  $R_\theta$  are about 21 mm, i.e.,  $\delta/H \approx 0.5$ , and 1200, respectively; for Case B,  $\delta$  and  $R_\theta$  are about 44 mm, i.e.,  $\delta/H \approx 1.1$ , and 3000, respectively. However, the Reynolds number based on the hill height is the same:  $Re_H = \bar{U}_0 H / \nu = 2.2 \times 10^4$ , in both cases.

In order to simulate the situation where the hill surface is locally heated by solar insolation, the thermal boundary condition is set as shown in Fig. 1. The model hill is composed of three parts: upstream and downstream flat plates of 2-mm-thick copper, and a curved plate made of 5-mm-thick copper. By controlling the heating current for heaters on the back side of the hill, we obtain uniform wall temperature distributions. The temperature difference between the wall and the ambient fluid is kept at about 10 K. It is confirmed that there are no effects on the flow field, even in the separated region. The static pressure holes (diameter: 0.5 mm) are drilled normal to the hill surface.

The velocities are measured by a backscatter-type two-component laser Doppler velocimetry (LDV) system (Dantec Dynamics). A water-cooled Argon ion laser (6W) is used as a light source. A focus length of the front lens is 300 mm, and the measurement volume is  $89.3 \mu\text{m} \times 1.41 \text{ mm}$  for green, and  $84.7 \mu\text{m} \times 1.34 \text{ mm}$  for blue. Seeding particles are generated by evaporating a SAFEX fog liquid, and introduced from the upstream of the settling chamber.

Fluid temperature is measured with a fine-wire thermocouple (chromel-alumel; diameter 13  $\mu\text{m}$ ; length 10 mm) and a cold-wire probe (platinum 90%/rhodium 10%; diameter 0.625  $\mu\text{m}$ ; length 1.0 mm). The response delay of the thermocouple is compensated using a scheme for a first-order lag system (Tagawa *et al.*, 2001, 2005).

## RESULTS AND DISCUSSION

### Pressure distribution

Figure 2 shows the distribution of the wall static pressure coefficient  $C_p = (\bar{P} - \bar{P}_0) / (\rho \bar{U}_0^2 / 2)$ . As explained in the previous section, the streamwise pressure gradient is set to zero, prior to the installation of the hill. Then, the hill's surface pressure is measured after the setup. From the results of  $C_p$  along the hill surface, a weak pressure rise (i.e., adverse pressure gradient) at the beginning of the windward slope (concave) follows a rapid favorable pressure gradient

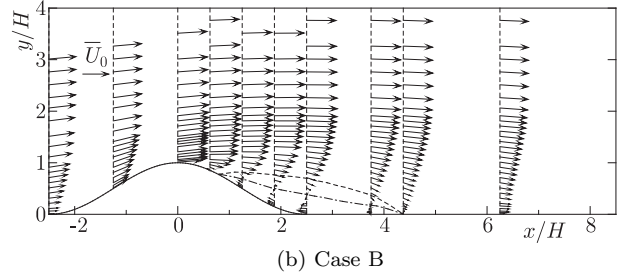
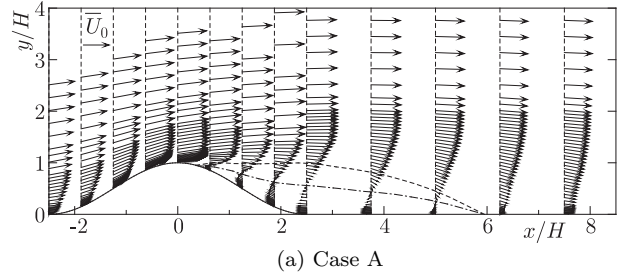


Figure 3: Mean velocity vectors around hill: (a) Case A; (b) Case B.

on the windward slope (convex) toward the crest of the hill, and then the adverse pressure gradient appears again in the reverse-flow and recovery regions on the leeward side. It should be noted that the wall static pressure shows a minimum before the crest, and then a plateau region along the leeward side of the hill. This pressure plateau is also observed in the LES study of periodic 2D hill (Fröhlich *et al.*, 2005); thus, this is considered to be one of general aspects in the separation region. Because of the pressure loss caused by a separation, the static pressure never regains the upstream value. The loss reaches about 5% of the free-stream dynamic pressure. There are slight differences between the two cases: if the ratio  $\delta/H$  is larger, the increase in the pressure is smaller in the approaching region. However, there are almost no effects in the downstream region.

### Velocity field

Figure 3 shows the mean velocity vectors around the hill. The dashed and chain lines respectively indicate the dividing streamline where the stream function equals zero and the forward-flow fraction becomes 50%. It is noted that the 50% line of forward-flow fraction almost corresponds to the zero-mean velocity ( $\bar{U}=0$ ) line. From this figure, on the windward slope of the hill, the velocity vectors change their directions along the surface, and the maximum velocity appears over the crest (see also Fig. 4 (a)). On the other hand, the reverse-flow region appears near the leeward side of the hill. The size of the separation bubble strongly depends on the ratio of the boundary layer thickness to the hill height,  $\delta/H$ . For Case A, the reattachment point  $x_R$  locates at about  $x_R/H \approx 6.0$ , whereas  $x_R/H \approx 4.4$  for Case B.

In order to investigate the effects of inflow boundary layer in more detail, Figs. 4 (a) and (b) show the horizontal and vertical mean velocity profiles on the windward side of the hill. The abscissa is the vertical distance from the hill surface normalized by the hill height,  $(y - h)/H$ . The mean velocities are normalized by the reference inlet velocity  $\bar{U}_0$ . On the windward side of the hill, after the  $C_p$  reaches maximum at  $x/H = -2.5$ , the horizontal mean velocity rapidly increases along the curved surface ( $x/H = -1.25$ ) to the crest of the hill ( $x/H = 0$ ). Although the inflow boundary

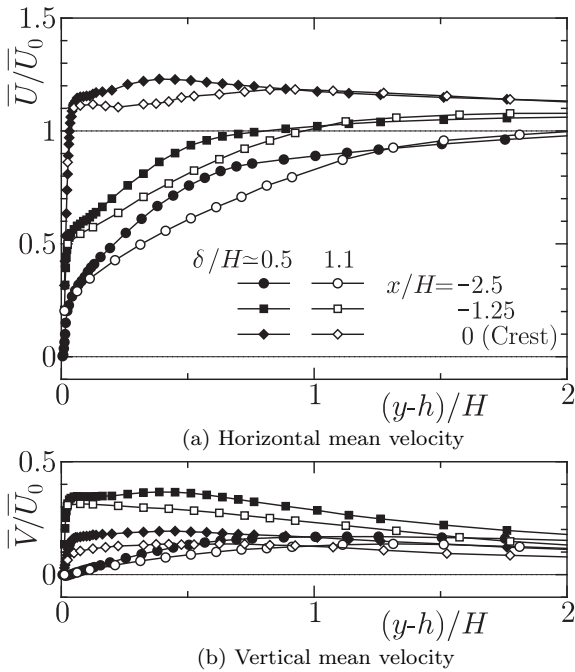


Figure 4: Mean velocity profiles on windward slope.

layer thickness definitely affects the mean velocity profiles as shown in Fig. 4, the difference in the horizontal mean velocity becomes smaller flowing downstream to the crest. On the other hand, the vertical mean velocity reaches maximum at the middle of the windward slope ( $x/H = -1.25$ ). And at the crest, the profile shows almost uniform distribution except very near the surface.

Figure 5 shows the turbulence intensities of the horizontal ( $u$ ) and vertical ( $v$ ) velocity fluctuations normalized by the reference inlet velocity  $\bar{U}_0$ . As seen from this figure, the developments of the intensities also depend on  $\delta/H$ . In order to investigate the intensity near the windward curved surface in detail, Fig. 6 (a) and (b) show the horizontal and vertical velocity fluctuations, respectively. When the inflow boundary layer is thick (Case B), the intensities extend in the vertical direction compared with a thinner case (Case A). Flowing downstream along the curved surface, the horizontal and vertical velocity fluctuations rapidly decrease with the increase in horizontal mean velocity. It is noted that very near the surface at the crest, horizontal velocity fluctuations show a large distinct peak. Because the instantaneous backward flows exist there, from the results of probability density functions (p.d.f.s), the instantaneous separation location moves back and forth. Thus, the separation point is not fixed on the crest of the two-dimensional hill model, unlike the case of backward-facing step flows. On the other hand, flowing downstream from the crest, the intensity of horizontal velocity fluctuation becomes maximum at the hill-top height, then gradually increases near the wall at the reattachment point (see Fig. 5). The intensity of the vertical fluctuation also reaches maximum at the hill top, whereas it is suppressed near the wall. After reattachment, this peak value gradually decreases in the streamwise direction. The turbulent production and redistribution processes among the velocity components should be strongly affected on the leeward side of the hill.

Figure 7 shows the Reynolds shear stress,  $-\overline{uv}$ , normalized by the reference inlet velocity  $\bar{U}_0$ . As seen from this figure, the Reynolds shear stress on the leeward side of the hill

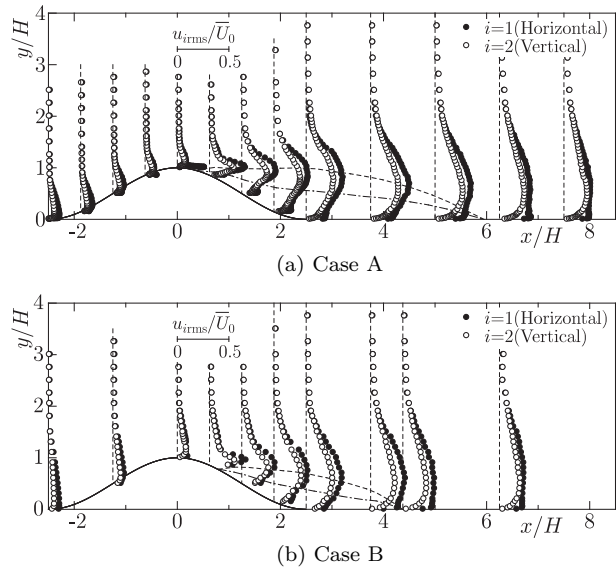


Figure 5: Horizontal and vertical turbulence intensities: (a) Case A; (b) Case B.

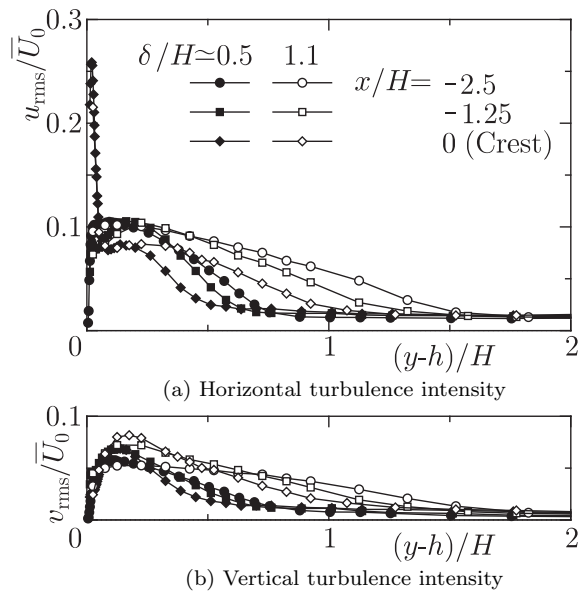


Figure 6: Profiles of horizontal and vertical turbulence intensities on windward slope.

has much higher values than those of a canonical wall flow, e.g., a maximum value of  $-\overline{uv}$  is typically  $0.002 \bar{U}_0^2$ . Moreover, the developments of the Reynolds shear stress strongly depend on  $\delta/H$ . Flowing downstream from the crest, the Reynolds shear stress becomes maximum at the hill top and is suppressed near the wall. After reattachment, their peak values gradually decrease in the streamwise direction. Figure 8 shows the ratios of the maximum Reynolds shear stress in the separated and reattaching regions ( $-\overline{uv})_{max}$  to that in a zero-pressure gradient flat-plate boundary layer ( $-\overline{uv})_{max,0}$ .

On the windward side of the hill, the most striking feature of the Reynolds shear stress is the positive value  $\overline{uv} > 0$ , near the surfaces of the middle slope and at the crest as shown in Fig. 9. On the other hand, the effects of the inflow boundary layer thickness on the Reynolds shear stress distributions are almost the same as those on the turbulence

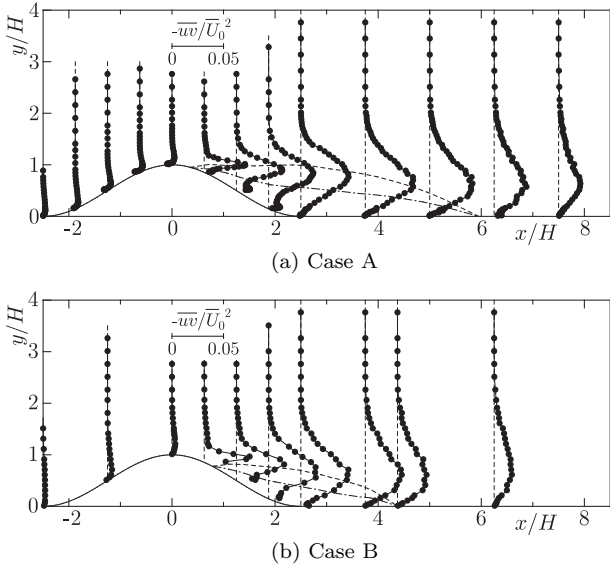


Figure 7: Reynolds shear stress,  $-\overline{w}$ : (a) Case A; (b) Case B.

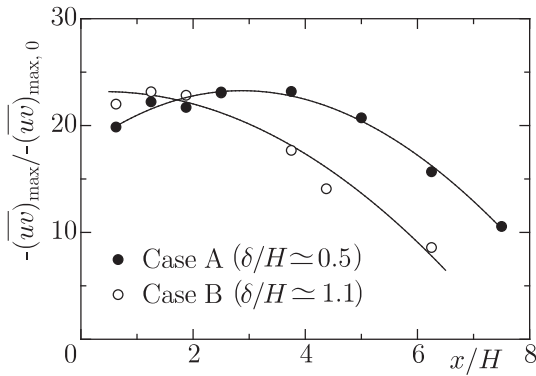


Figure 8: Ratio of maximum Reynolds shear stress in separated and reattaching regions to that in zero-pressure gradient flat-plate boundary layer.

intensities. Because the mean velocity vectors are tilted upward by the presence of the hill surface, the above discussion based on the wind tunnel coordinate  $(x, y)$  may cause misunderstanding of the turbulence field especially near the hill surface. Thus, in the following we discuss the statistical results based on the local mean velocity coordinate,  $(x_s, y_s)$ , defined below.

The local angle to the Cartesian coordinate is defined as:  $\theta = \tan^{-1}(\overline{V}/\overline{U})$ . Then, the Reynolds shear stress based on the local mean velocity coordinate is estimated as:

$$\overline{u_s v_s} = \cos(2\theta) \overline{u v} + \sin(2\theta) (\overline{v^2} - \overline{u^2}) / 2. \quad (2)$$

These Reynolds shear stress are compared based on the different coordinates as shown in Fig. 10. As seen from this figure, the positive sign near the surface disappears in the local coordinate. Figure 11 shows the joint p.d.f.s based on the two coordinates. The joint p.d.f.s are defined as follows:

$$1 = \iint_{-\infty}^{\infty} P(u', v') du' dv' = \iint_{-\infty}^{\infty} P(u'_s, v'_s) du'_s dv'_s, \quad (3)$$

where each instantaneous velocity fluctuation is normalized by  $\overline{U}_0$ , i.e.  $u' = u/\overline{U}_0$  and  $v' = v/\overline{U}_0$ . As seen from Fig. 11

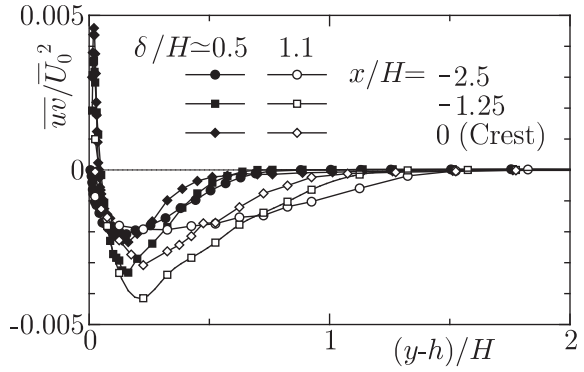


Figure 9: Reynolds shear stress profiles on windward slope.

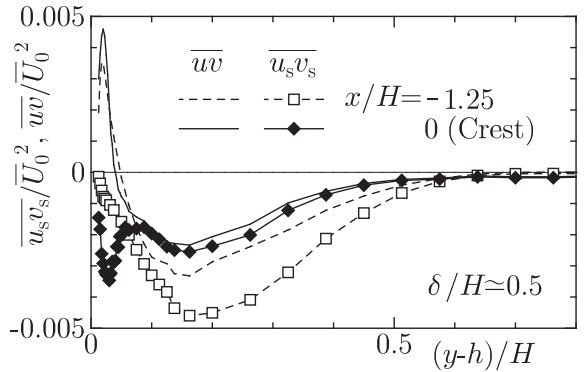


Figure 10: Reynolds shear stress profiles on windward slope based on the Cartesian and local mean velocity coordinates.

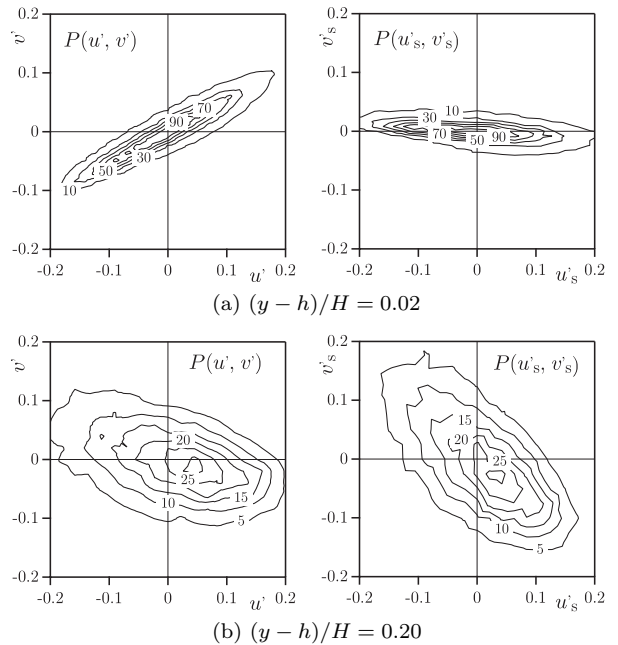
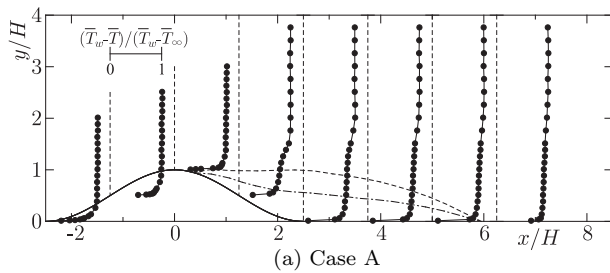
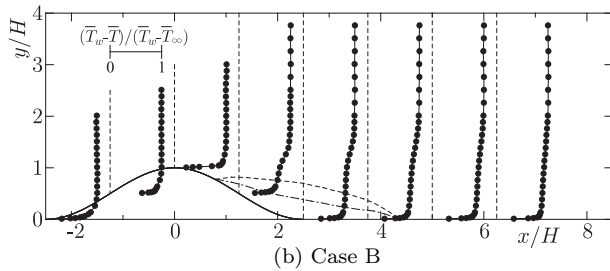


Figure 11: Joint probability density functions of  $u$  and  $v$  on windward slope (Case A:  $\delta/H \approx 0.5, x/H = -1.25$ ).

(a), very near the surface the  $P(u', v')$  shows strong *positive* correlation between  $u$  and  $v$  (see also Fig. 10). In the local coordinate, however, the  $P(u'_s, v'_s)$  shows a *negative* correlation as is generally seen in a canonical wall shear flow.



(a) Case A



(b) Case B

Figure 12: Mean temperature: (a) Case A; (b) Case B.

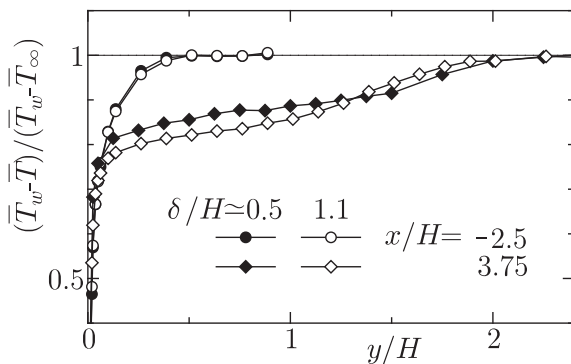
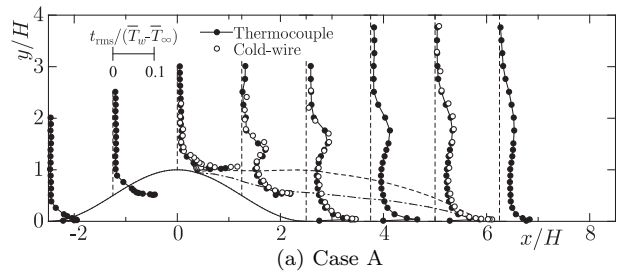


Figure 13: Mean temperature profiles at upstream and separated regions.

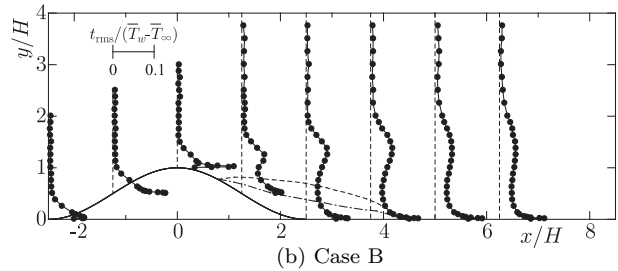
**Temperature field**

Finally, we discuss the effects of the inflow boundary layer on the temperature field. Figure 12 shows the mean temperature profiles normalized by the temperature difference between the wall,  $\bar{T}_w$ , and the ambient,  $\bar{T}_\infty$ . As seen from the figure, on the windward side of the hill, the thermal boundary layer thickness at the crest ( $x/H = 0$ ) is thinner than that of the upstream one because of the strong acceleration of the flow on the windward slope. Flowing downstream from the crest, flow separation occurred, so the mean temperature shows a peculiar profile; it is kept relatively high around the separation region, and then rapidly decreases to an ambient temperature above the hill height. Thus, there is a local maximum of the mean temperature gradient, besides the heated surface near the wall. The maximum location moves away from the heated wall in the downstream direction for Case A. On the other hand, for Case B, the location remains at a nearly constant distance from the wall.

In order to clarify the effects of the inflow boundary layer, Fig. 13 shows the mean temperature profiles at the upstream ( $x/H = -2.5$ ) and separated ( $x/H = 3.75$ ) regions. In the upstream region, the thickness of the thermal boundary layer is about half of the hill height in both cases. And there are no distinct differences between two cases. In the separated region, the hot region is below the hill height in both cases. However, the hot region is larger for Case A than Case B, possibly due to the differences in the velocity field.



(a) Case A



(b) Case B

Figure 14: Intensity of temperature fluctuation: (a) Case A; (b) Case B.

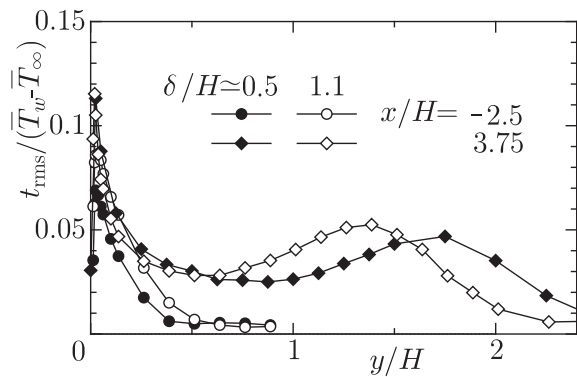


Figure 15: Intensity of temperature fluctuation at upstream and separated regions.

Next, Fig. 14 shows the intensity profiles of temperature fluctuation. The response delay of the thermocouple is compensated using a scheme for a first-order lag system (Tagawa *et al.*, 2001, 2005). Then, the temperature-fluctuation results obtained by the thermocouple agree well with those by a fine cold-wire. As discussed in the mean temperature profiles, the gradient has peaks in the hill-height location as well as at the heated surface. Thus, because the velocity fluctuation exists where the gradient is large, there is a second peak of temperature fluctuation except near the heated surface. The second peak location moves away from the hill-height location in the downstream direction for Case A. On the other hand, for Case B, the location remains at a nearly constant distance from the wall.

In order to investigate the effects of the thickness of the inflow boundary layer in detail, the distribution of the temperature fluctuation intensity is shown in Fig. 15. Though hardly any difference is seen in the mean temperature distribution upstream of the hill, the temperature fluctuation intensity is larger, when the boundary layer is thick (Case B). In the separated region, the position of the second peak is farther for Case A than for Case B. The thickness of the inflow boundary layer is small in Case A. However, the separation bubble is large, and the range where the influence of the temperature distribution reaches is wider.

## CONCLUSIONS

In the present paper, an experimental investigation is made on the flow and thermal fields over a heated two-dimensional hill. The effects of the inflow boundary layer on the complex turbulent field are discussed when the downstream location of the hill model is varied.

It is found that in the reverse-flow region on the leeward side of the hill, the turbulence intensities and the Reynolds shear stress show much larger values than those in a canonical wall-bounded shear flow. The ratio  $\delta/H$  strongly affects the development of these turbulent statistics. The horizontal velocity fluctuation shows a large distinct peak very near the surface at the crest. Because the instantaneous backward flows exist there, the instantaneous separation location moves back and forth. The separation point is not fixed on the crest of the two-dimensional hill model, unlike the case of backward-facing step flows.

On the leeward side of the hill, the turbulent production and redistribution processes among the velocity components should be very sensitive to the ratio  $\delta/H$ . In the thermal field, there is a hot region below the hill height, and the mean temperature gradient has peaks at this location as well as at the heated surface. Then, there is a second temperature fluctuation peak except near the heated surface.

## ACKNOWLEDGEMENTS

This work was supported by Grant-in-Aid for Scientific Research (S) (No. 17106003) from the Japan Society for the Promotion of Science (JSPS).

## REFERENCES

- Almeida, G.P., Durão, D.F.G. and Heitor, M.V., 1993, "Wake flows behind two-dimensional model hills," *Exp. Therm. Fluid Sci.*, Vol. 7, pp. 87-101.
- Britter, R.E., Hunt, J.C.R. and Richards, K.J., 1981, "Air flow over a two-dimensional hill: studies of velocity speed-up, roughness effects and turbulence," *Quart. J. R. Met. Soc.*, Vol. 107, pp. 91-110.
- Ferreira, A.D., Silva, M.C.G., Viegas, D.X. and Lopes, A.G., 1991, "Wind tunnel simulation of the flow around two-dimensional hills," *J. Wind Eng. Ind. Aero.*, Vol. 38, pp. 109-122.
- Ferreira, A.D., Lopes, A.M.G., Viegas, D.X. and Sousa, A.C.M., 1995, "Experimental and numerical simulation of flow around two-dimensional hills," *J. Wind Eng. Ind. Aero.*, Vols. 54-55, pp. 173-181.
- Fröhlich, J., Mellen, C.P., Rodi, W., Temmerman, L. and Leschziner, M.A., 2005, "Highly resolved large-eddy simulation of separated flow in a channel with streamwise periodic constrictions," *J. Fluid Mech.*, Vol. 526, pp. 19-66.
- Gong, W. and Ibbetson, A., 1989, "A wind tunnel study of turbulent flow over model hills," *Boundary-Layer Meteorology*, Vol. 49, pp. 113-148.
- Hattori, Y. and Tanaka, N., 2006, "A wind tunnel experiment of inflow turbulence effects on development of turbulent boundary layer over a steep hill," *Proc. 17th Int. Symposium on Transport Phenomena*, Toyama, Japan, CD-ROM, 6 pages.
- Houra, T., Tagawa, M. and Nagano, Y., 2008, "Turbulent heat and fluid flow over a two-dimensional hill," *7th International ERCOFTAC Symposium on Engineering Turbulence Modelling and Measurements (ETMM7)*, Limassol, Cyprus, pp. 268-273.
- Hunt, J.C.R. and Snyder, W.H., 1980, "Experiments on stably and neutrally stratified flow over a model three-dimensional hill," *J. Fluid Mech.*, Vol. 96, pp. 671-704.
- Kim, H.G., Lee, C.M. and Lim, H.C. and Kyong, N.H., 1997, "An experimental and numerical study on the flow over two-dimensional hills," *J. Wind Eng. Ind. Aero.*, Vol. 66, pp. 17-33.
- Loureiro, J.B.R., Pinho, F.T. and Silva Freire, A.P., 2007, "Near wall characterization of the flow over a two-dimensional steep smooth hill," *Exp. Fluids*, Vol. 42, pp. 441-457.
- Ross, A.N., Arnold, S., Vosper, S.B., Mobbs, S.D., Dixon, N. and Robins, A.G., 2004, "A comparison of wind-tunnel experiments and numerical simulations of neutral and stratified flow over a hill," *Boundary-Layer Meteorology*, Vol. 113, pp. 427-459.
- Tagawa, M., Nagaya, S. and Ohta, Y., 2001, "Simultaneous measurement of velocity and temperature in high-temperature turbulent flows: a combination of LDV and a three-wire temperature probe," *Exp. Fluids*, Vol. 30, pp. 143-152.
- Tagawa, M., Kato, K. and Ohta, Y., 2005, "Response compensation of fine-wire temperature sensors," *Rev. Sci. Instrum.*, Vol. 76, 094904.
- Taylor, P.A., Mason, P.J. and Bradley, E.F., 1987, "Boundary-layer flow over low hills," *Boundary-Layer Meteorology*, Vol. 39, pp. 107-132.
- Wood, N., 1995, "The onset of separation in neutral, turbulent flow over hills," *Boundary-Layer Meteorology*, Vol. 76, pp. 137-164.